AGU PUBLICATIONS

JGR

Journal of Geophysical Research: Atmospheres

RESEARCH ARTICLE

10.1002/2013JD021205

Key Points:
- Temporal sampling biases are smaller than instrumental sampling biases
- Sampling biases are smaller than measurement uncertainties
- AIRS/AMSU-A and MERRA climatologies do not always agree

Supporting Information:
- Readme
- Figure S1
- Figure S2
- Figure S3
- Figure S4
- Figure S5

Correspondence to:
T. J. Hearty,
thomas.hearty@nasa.gov

Citation:
Hearty, T. J., A. Savtchenko, B. Tian, E. Fetzer, Y. L. Yung, M. Theobald, B. Vollmer, E. Fishbein, and Y.-I. Won (2014), Estimating sampling biases and measurement uncertainties of AIRS/AMSU-A temperature and water vapor observations using MERRA reanalysis, *J. Geophys. Res. Atmos.*, *119*, 2725–2741, doi:10.1002/2013JD021205.

Received 14 NOV 2013
Accepted 11 FEB 2014
Accepted article online 14 FEB 2014
Published online 18 MAR 2014

Estimating sampling biases and measurement uncertainties of AIRS/AMSU-A temperature and water vapor observations using MERRA reanalysis

Thomas J. Hearty[1], Andrey Savtchenko[2], Baijun Tian[3], Eric Fetzer[3], Yuk L. Yung[4], Michael Theobald[2], Bruce Vollmer[5], Evan Fishbein[3], and Young-In Won[1]

[1]Goddard Space Flight Center/Wyle, Greenbelt, Maryland, USA [2]Goddard Space Flight Center/ADNET, Greenbelt, Maryland, USA [3]Jet Propulsion Laboratory/California Institute of Technology, Pasadena, California, USA, [4]Division of Geological and Planetary Sciences, California Institute of Technology, Pasadena, California, USA [5]Goddard Space Flight Center, Greenbelt, Maryland, USA

Abstract We use MERRA (Modern Era Retrospective-Analysis for Research Applications) temperature and water vapor data to estimate the sampling biases of climatologies derived from the AIRS/AMSU-A (Atmospheric Infrared Sounder/Advanced Microwave Sounding Unit-A) suite of instruments. We separate the total sampling bias into *temporal* and *instrumental* components. The temporal component is caused by the AIRS/AMSU-A orbit and swath that are not able to sample all of time and space. The instrumental component is caused by scenes that prevent successful retrievals. The temporal sampling biases are generally smaller than the instrumental sampling biases except in regions with large diurnal variations, such as the boundary layer, where the temporal sampling biases of temperature can be $\pm$ 2 K and water vapor can be 10% wet. The instrumental sampling biases are the main contributor to the total sampling biases and are mainly caused by clouds. They are up to 2 K cold and > 30% dry over midlatitude storm tracks and tropical deep convective cloudy regions and up to 20% wet over stratus regions. However, other factors such as surface emissivity and temperature can also influence the instrumental sampling bias over deserts where the biases can be up to 1 K cold and 10% wet. Some instrumental sampling biases can vary seasonally and/or diurnally. We also estimate the combined measurement uncertainties of temperature and water vapor from AIRS/AMSU-A and MERRA by comparing similarly sampled climatologies from both data sets. The measurement differences are often larger than the sampling biases and have longitudinal variations.

1. Introduction

Earth observations by satellite are becoming more accurate, more abundant, and easier to access and can serve as valuable resources for evaluating climate models. The AIRS/AMSU-A (Atmospheric Infrared Sounder/Advanced Microwave Sounding Unit-A [*Aumann et al.*, 2003]) suite of instruments has decadal observations of atmospheric temperature and water vapor which are included in the Obs4MIPs (Observations for Model Intercomparison Projects) program [e.g., *Tian et al.*, 2013]. However, one of the greatest challenges of using satellite observations from Low Earth Orbit (LEO) to evaluate climate models is to account for differences in the sampling. Climate models sample natural variability on a regular grid in time and space while LEO satellite observations do not. Since AIRS is on the Aqua spacecraft in a Sun-synchronous LEO with a limited swath width, its sampling of the diurnal cycle and synoptic events is incomplete. Moreover, since the AIRS is an infrared instrument, its sampling is affected by clouds, aerosols, coastlines, and other factors that affect its ability to perform successful retrievals. These sampling differences can affect comparisons with climate models [e.g., *Tian et al.*, 2013]. Therefore, we consider two components to the total sampling bias of an AIRS/AMSU-A climatology:

1. The *temporal* component is caused by the Aqua spacecraft's Sun-synchronous low Earth orbit and the limited swath width of the AIRS/AMSU-A instruments that results in undersampling temporal (especially diurnal) and spatial variations.
2. The *instrumental* component caused by the quality control imposed in regions where the AIRS/AMSU-A instrument suite or algorithm is not able to successfully perform a retrieval.

Numerous authors [e.g., *Guan et al.*, 2013; *Kirk-Davidoff et al.*, 2005; *Lin et al.*, 2002; *Leroy*, 2001; *Fowler et al.*, 2000; *Bell and Kundu*, 1996; *North et al.*, 1993] have discussed temporal sampling biases (What we call

temporal sampling biases are sometimes referred to as orbital sampling biases or just sampling biases when other effects can be neglected.). However, it is also important to understand the instrumental sampling biases when an instrument or algorithm is not sensitive to certain atmospheric states. *Tian et al.* [2013] show that sampling data from MERRA (Modern Era Retrospective-Analysis for Research Applications [*Rienecker et al.*, 2011]), a product of GEOS-5 (Goddard Earth Observing System Model, Version 5) Data Assimilation System that includes model and assimilation data, with different cloud amounts can alter the yearly averages of temperature and water vapor. *Tian et al.* [2013] have also shown that the differences between climatological means of AIRS/AMSU-A and MERRA specific humidity are mainly located in deep convective cloudy regions such as the ITCZ (Intertropical Convergence Zone), the SPCZ (South Pacific convergence zone), and midlatitude storm tracks and speculate that these regions may contain a significant clear sky sampling bias. Their speculations are consistent with other studies that have shown differences between infrared and microwave observations which have different sampling rates [e.g., *Fetzer et al.*, 2006; *John et al.*, 2011]. It is important to understand these biases when creating a climatology from this type of observation to evaluate climate models since the models have very different sampling. We use MERRA temperature and water vapor data to estimate the sampling bias of a climatology derived from AIRS/AMSU-A observations by examining differences between MERRA climatologies with different sampling assuming that the MERRA data correctly samples the atmospheric state.

We derive sampling bias estimates for AIRS/AMSU-A, however, any Earth-observing instrument in a Sun-synchronous low Earth orbit with a 1:30 A.M./P.M. equator crossing time would have similar temporal biases that may be larger or smaller depending upon the swath width. Also, similar instrumental sampling biases likely exist for other infrared instruments (e.g., The Moderate Resolution Imaging Spectroradiometer (MODIS), the Infrared Atmospheric Sounding Interferometer (IASI), and the Cross-track Infrared Sounder (CrIS)).

The AIRS/AMSU-A and MERRA data sets are both being used to evaluate climate models [e.g., *Tian et al.*, 2013 and *Fasullo and Trenberth*, 2012]; therefore, it is important to understand how these data sets differ independently of sampling. For example, *Susskind et al.* [2006] show a slight decrease in the accuracy of AIRS/AMSU-A retrievals with increasing cloud cover. We estimate the residual *measurement* errors by calculating the differences between temperature and water vapor climatologies created from AIRS/AMSU-A observational data and from similarly sampled MERRA data. This allows separation of the differences due to sampling from differences when AIRS/AMSU-A is able to obtain observations. The differences between AIRS/AMSU-A temperature and water vapor climatologies and the similarly sampled MERRA climatologies serve as a combined measurement uncertainty in the regions where AIRS/AMSU-A is able to obtain observations.

Section 2 describes how we use AIRS/AMSU-A and MERRA data to estimate the sampling biases of AIRS/AMSU-A temperature and water vapor climatologies and the combined measurement uncertainties of AIRS/AMSU-A and MERRA climatologies. Section 3 describes our estimates based on MERRA of the total, temporal, and instrumental components to the sampling biases of AIRS/AMSU-A temperature and water vapor climatologies. Section 4 presents the combined measurement uncertainties by comparing AIRS/AMSU-A and MERRA data with similar sampling to assess how well the satellite observations and reanalysis temperature and water vapor agree independent of sampling effects. Section 5 presents several limitations of our study. Section 6 summarizes our findings.

2. Data and Analysis

2.1. AIRS/AMSU-A Observations and Climatology

The AIRS/AMSU-A suite of instruments observes Earth from aboard the Aqua spacecraft at an altitude of ~705 km in a near-polar Sun-synchronous orbit with an inclination of 98.2° [*Parkinson*, 2003]. The ascending nodes of the orbit (i.e., when the spacecraft is moving toward the north) correspond to daytime observations (~1:30 P.M. local time) near the equator and the descending nodes of the orbit (when the spacecraft is moving toward the south) correspond to nighttime observations (~1:30 A.M. local time) near the equator. The AIRS/AMSU-A instruments scan ± 49° about nadir with a swath width of ~1650 km [*Aumann et al.*, 2003]. Because of the wide swath, the local time of data collection along the equator can be between 12:50–2:10 P.M. and 12:50–2:10 A.M.for the ascending and descending parts of the orbit, respectively. The time range of data collection broadens closer to the poles so that the 98.8 minute orbit can sample the poles 14 or 15 times per day [*Parkinson*, 2003]. The instruments have 2378 channels in the wavelength range from

3.75 to 15.4 μm ($\lambda/\delta\lambda \sim 1200$) and 15 channels from 23.8 to 89 GHz. The AIRS/AMSU-A science team retrieval algorithm uses both AIRS and AMSU-A data to infer temperature and water vapor profiles of the atmosphere [*Susskind et al.*, 2011, 2003].

We use level 2 data from version 5 of the AIRS/AMSU-A science team algorithm to create 9 year temperature and water vapor climatologies. We generate the AIRS/AMSU-A climatologies by calculating the arithmetic mean of the AIRS/AMSU-A level 2 temperature and water vapor estimates from the AIRX2RET product over 9 years of observations on a 1° × 1° grid in a manner analogous to the version 5 monthly mean AIRS/AMSU-A level 3 data [*Olsen et al.*, 2007]. Specifically, we create the AIRS/AMSU-A temperature and water vapor climatologies as follows:

1. We average together AIRS/AMSU-A level 2 monthly means of temperature and water vapor profile data on a 1°×1° grid for each grid point over a 9 year period from September 2002 to August 2011. We average data from both the ascending and descending orbital nodes with equal weight given to each node rather than separately averaging the nodes as is done for the AIRS/AMSU-A level 3 standard product.
2. We include all data for which the retrieval is either "good" or "best" according to the AIRS/AMSU-A quality control without regard as to whether it is over land, ocean, or coastline. This gives us a slightly higher yield than the standard version 5 AIRS/AMSU-A level 3 which defines each grid point as either land or ocean and only includes observations of that type;
3. We correct an error in the version 5 level 3 code that sometimes allows nonphysical temperatures near the surface. Although it may affect all near-surface temperature measurements, it is most noticeable near steep topography such as the Andes and the Tibetan Plateau where the AIRS version 5 level 3 product sometimes reports unrealistically high air temperatures.

2.2. MERRA Data

We create the 9 year MERRA climatologies by averaging temperature and water vapor profile data from the MERRA Incremental Analysis Update 3-D assimilated state ("inst3_3d_asm_Cp" also known as "MAI3CPASM") produced from version 5 of the GEOS Data Assimilation System that assimilates numerous types of observations (e.g., radiosonde, ground station, and satellite) and includes model calculations. The MAI3CPASM data are provided on a 1.25° × 1.25° grid with 42 vertical levels in pressure and sampled every 3 h in time. Since the MERRA data have a vertical grid point for each of the AIRS/AMSU-A standard temperature levels, we use the MERRA temperature from the same level as the AIRS/AMSU-A observation. Since the MERRA water vapor is provided as a *level* specific humidity we convert it to a *layer* mixing ratio to match the AIRS/AMSU-A data by first converting the MERRA specific humidity to a mixing ratio and then interpolating the MERRA value to the geometric mean pressure of the AIRS/AMSU-A layer. Although the interpolation may produce a bias, it would be canceled out when calculating the difference between climatologies created from MERRA both of which are interpolated in the same way. However, it may produce biases in our comparisons of similarly sampled MERRA and AIRS/AMSU-A climatologies.

2.3. Methodology for Calculating the Sampling Bias and Uncertainty Estimates

We use the differences between MERRA temperature and water vapor climatologies with different sampling to estimate the sampling biases of an AIRS/AMSU-A climatology. The MERRA climatologies for this analysis are created by sampling MERRA data in three different ways:

1. A MERRA sampled like AIRS/AMSU-A (hereafter, MSA) climatology is created with MERRA data sampled like AIRS/AMSU-A in space and time but without applying the AIRS quality control. We resample the MERRA data to be like AIRS/AMSU-A by using the MERRA data nearest in time (UTC) and space (longitude and latitude) to each AIRS/AMSU-A level 2 observation and then average the data onto a 1° × 1° grid like that of the AIRS/AMSU-A level 3 product with the few differences described in section 2.1. Since the MERRA grid has a coarser spatial resolution than the AIRS/AMSU-A level 2 observations, we allow MERRA profiles to be distributed over multiple AIRS/AMSU-A level 2 locations but the AIRS coordinates are used when averaging onto the 1° × 1° grid.
2. A MERRA sampled like AIRS/AMSU-A with Quality Control (hereafter, MSAQC) climatology is created with MERRA data sampled like AIRS/AMSU-A in space and time including AIRS/AMSU-A quality control. This climatology is similar to the MSA climatology; however, the data is selected for gridding based on the AIRS level 2 quality flags in addition to the space and time constraints. We use the same quality criteria as used for generating the AIRS/AMSU-A level 3 standard product (i.e., we only include data flagged as "best" or "good"). Specifically, when creating the temperature climatology we only include temperature estimates

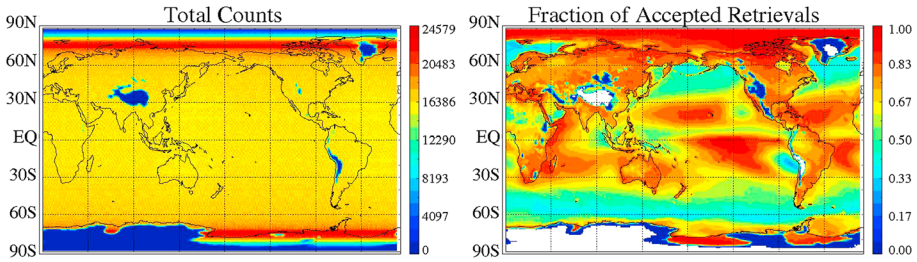

Figure 1. (left) The number of attempted AIRS temperature retrievals at 850 hPa that are included in the 9 year average climatology. (right) The fraction of attempted retrievals that were accepted by the AIRS/AMSU-A quality control algorithm.

for pressures less than or equal to (i.e., above in altitude) the maximum value of the pressure for which the temperature is of the "best" or "good" quality, Pressure Good (PGood). When creating the water vapor climatology we only include water vapor estimates for which there is a valid AIRS/AMSU-A measurement and for which the overall quality flag for water vapor, Quality H_2O (Qual_H2O) is 0 or 1, meaning the data are of the "best" or "good" quality.

3. A MERRA Monthly Mean (hereafter, MMM) climatology is created over the same 9 year epoch as AIRS/AMSU-A but from the MERRA "MAIMCPASM" monthly product that includes the full diurnal variation sampled every 3 h at every grid point. Since this climatology is not sampled like AIRS, we just average the temperature and water vapor data from the MERRA monthly mean files over the same 9 year time period after regridding the data to a 1° × 1° grid. We also refer to this as the MERRA climatology sampled like a climate model.

Figure 1 illustrates the sampling of the 850 hPa temperature in the MSA and MSAQC climatologies. The sampling of the MSA climatology is a function of the orbit, the scan pattern, and the topography. The scans from adjacent orbits overlap closer to the poles, therefore the "counts" (i.e., number of attempted retrievals) shown in Figure 1 (left) increase near the poles. However, since the orbit is near-polar (rather than polar), the peak in the number of counts is slightly offset from the poles. The number of counts at 850 hPa (Figure 1) also decreases in regions of high terrain where the surface pressure is less than 850 hPa, and thus, the atmosphere can never be sampled at this level. In addition to the orbit, the scan pattern, and the topography, the sampling of the MSAQC climatology is also a function of the quality control. We emphasize how quality control influences sampling in Figure 1 (right) by showing the fraction of the number of accepted retrievals over the number of attempted retrievals for each grid cell. Since this ratio has a similar spatial pattern to the distribution of cloud amount [cf. *Rossow and Schiffer*, 1991, Plate 1], we infer that much of the instrumental sampling bias is caused by clouds. This is consistent with the conclusion from *Tian et al.* [2013]. However, in section 4 we show that surface emissivity, temperature, and Sun glint may also affect instrumental sampling in some regions.

We use differences between the MERRA climatologies described above to estimate the total, temporal, and instrumental sampling bias components of AIRS/AMSU-A temperature and water vapor climatologies. The differences between the MSAQC and the MMM climatologies provide estimates of the *total* sampling biases of an AIRS/AMSU-A climatology. The differences between the MSA and MMM climatologies provide estimates of the temporal sampling biases of an AIRS/AMSU-A climatology. The differences between the MSAQC and the MSA climatologies provide estimates of the instrumental sampling biases of an AIRS/AMSU-A climatology. The climatological differences we use for calculating the components to the sampling bias are summarized in Table 1.

Table 1. Climatology Differences Used for Sampling Bias Estimates

Bias Component	Climatology Difference[a]
Total	MSAQC-MMM
Temporal	MSA-MMM
Instrumental	MSAQC-MSA

[a]Abbreviations: MSA = MERRA sampled like AIRS/AMSU-A; MSAQC = MERRA sampled like AIRS/AMSU-A with Quality Control; MMM = MERRA Monthly Mean.

Since the MMM climatology is generated from the 3-hourly MERRA files, it is already sensitive to the full diurnal cycle (insofar as MERRA is sensitive to diurnal variability). Therefore, we average the MSA and MSAQC climatologies over the ascending (daytime) and descending (nighttime) nodes of

the AIRS/AMSU-A orbit with equal weights given to each node for comparisons with the MMM climatology to crudely estimate the full diurnal cycle.

The quality flags used to generate the MSAQC climatologies can be influenced by a myriad of atmospheric phenomena that vary seasonally and diurnally. Therefore, we examine the seasonal and diurnal variations of the instrumental sampling bias by calculating the differences between MSAQC and MSA climatologies independently for the ascending (daytime) and descending (nighttime) parts of the orbit and for each of four seasons (e.g., December, January, and February, March, April, and May, etc.), in addition to the yearly average climatologies. We refer to the orbitally and seasonally averaged versions of the climatologies with orbital and seasonal designations (e.g., "MSAQC-A-DJF" is the "MSAQC" climatology for the ascending "A" part of the orbit during the December, January, and February "DJF" seasons) to distinguish them from the versions that are averaged over the ascending and descending parts of the orbit for all seasons.

We estimate the combined measurement uncertainties of AIRS/AMSU-A and MERRA in regions where AIRS/AMSU-A is able to obtain observations by calculating the difference between AIRS/AMSU-A and MSAQC climatologies of temperature and water vapor. However, further validation studies of the regions where significant differences are noted is necessary to determine whether the AIRS/AMSU-A or the MERRA estimates are more accurate. Thus, we refer to these differences as combined measurement uncertainties of AIRS/AMSU-A and MERRA climatologies rather than biases.

2.4. Significance Testing

We estimate the significance of the differences between the climatologies using a paired Student's *t* test. Calculating the standard deviation of the difference between paired months reduces the influence nonnormal seasonal and interannual variations have on our significance estimates. The hypothesis tested is that the analyzed differences are null at the 95% confidence level. When this hypothesis is rejected, the differences are significant at the 95% confidence level. We only show differences that exceed the 95% confidence level in the climatological difference maps.

3. Sampling Biases

We use the differences between MSAQC, MSA, and MMM temperature and water vapor climatologies as shown in Table 1 to estimate the total (section 3.1), temporal (section 3.2), and instrumental (section 3.3) components to the sampling bias of AIRS/AMSU-A temperature and water vapor climatologies.

3.1. Total Sampling Bias

Figure 2 shows our estimate based on MERRA of the yearly average total temperature and water vapor sampling biases of an AIRS/AMSU-A climatology for the standard levels/layers up to 300 hPa. Although there are seasonal variations in the total sampling bias, they are mainly due to instrumental effects which we examine in section 3.3. The striking similarity of Figure 2 and *Tian et al.* [2013, Figures 7, 9, and 10], which includes both sampling and measurement differences, indicates that in many regions the differences between AIRS/AMSU-A and MERRA climatologies from *Tian et al.* [2013] can be attributed to AIRS/AMSU-A sampling biases.

The sampling biases tend to be both cold (up to 2 K) and dry (up to 30%) throughout the troposphere over the midlatitude storm tracks (Figure 2). The sampling biases of the AIRS/AMSU-A water vapor also tend to be dry (up to 30%) over the tropical convective cloudy regions, such as the ITCZ, SPCZ, western Pacific warm pool, equatorial south America, and south Atlantic convergence zone. However, the sampling bias is wet over the ocean off the west coast of South America and southern Africa between 850 and 500 hPa. These findings are consistent with *Fetzer et al.* [2006] who observe that an AIRS/AMSU-A total water vapor climatology has a dry bias over storm tracks and a wet bias over stratus regions compared to a climatology from AMSR-E (Advanced Microwave Scanning Radiometer for Earth Observing System) which is less sensitive to clouds.

Over the Sahara, Sahel, and the Arabian Peninsula there is a cold bias at 850 hPa and a wet bias that extends vertically throughout the troposphere (Figure 2). Figure 2 also shows that the boundary layer temperature has both warm and cold biases that are mainly located in the temperate zones and the arctic. The boundary layer water vapor over the ocean in the tropics and subtropics has a wet bias that is largest close to some coastlines and a dry bias at higher latitudes.

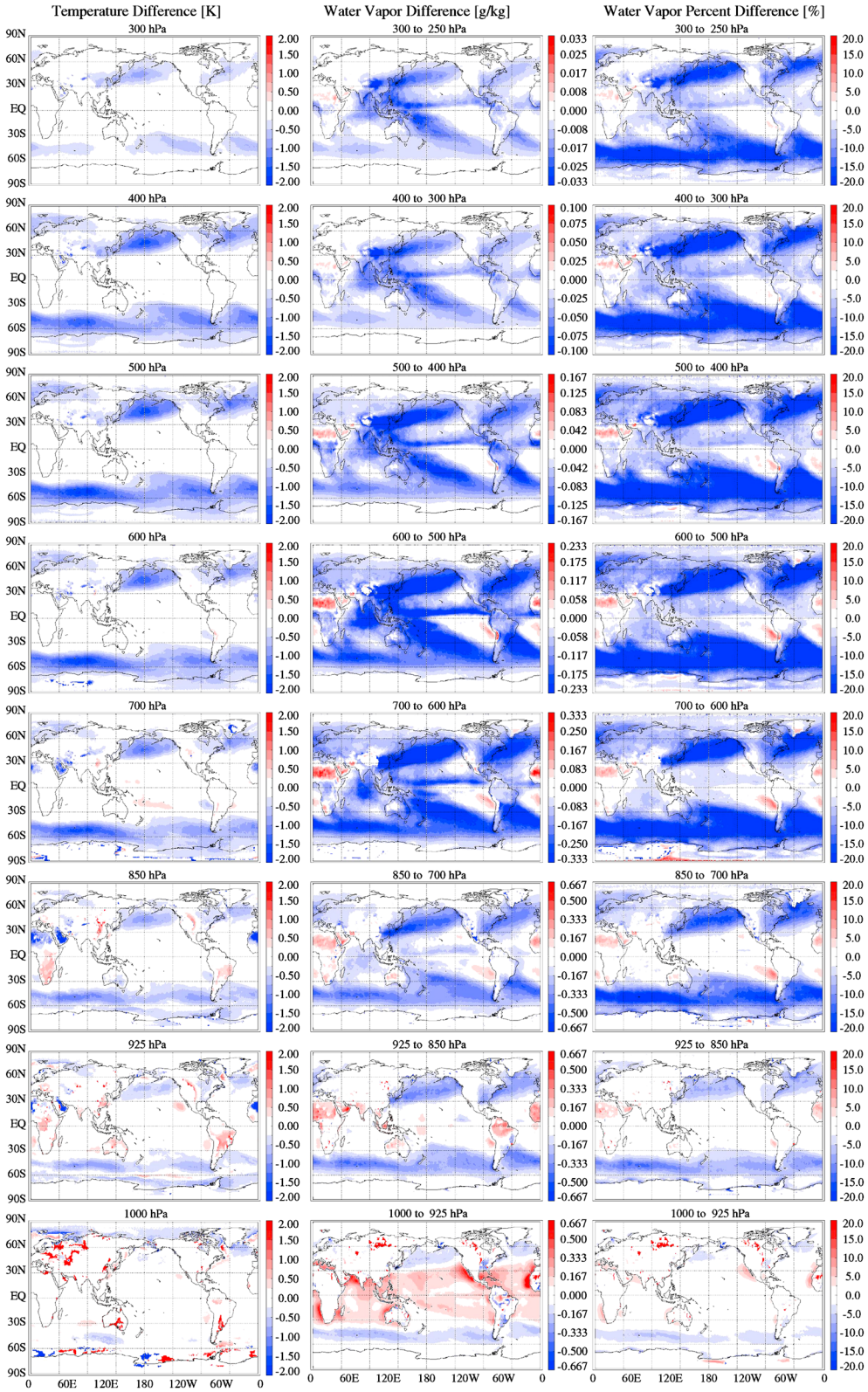

Figure 2. Differences between MERRA sampled Like AIRS/AMSU-A with Quality Control minus MERRA Monthly Mean climatologies (i.e., MSAQC-MMM) of temperature in Kelvins, water vapor in g/kg, and water vapor percent difference are displayed from left to right. This is an estimate of the total sampling bias of an AIRS/AMSU-A climatology that includes both the temporal and instrumental components to the sampling bias.

Table 2. Total Sampling Bias Estimates

Region	Bias	Reason[a]
Troposphere above temperate zones	up to 2 K cold and > 20% dry (larger over oceans)	I
Troposphere above 850 hPa in the ITCZ and SPCZ	up to 20% dry	I
Boundary layer water vapor above tropical and subtropical ocean	up to 10% wet (larger close to continents)	T
Boundary layer Temperature	± 2 K	T and I
Sahara, Sahel, and the Arabian Peninsula at 850 hPa	up to 2 K cold	I
Troposphere above the Sahara, Sahel, and the Arabian Peninsula	up to 15% Wet	I

[a]T = Temporal, I = Instrumental.

We summarize the total sampling biases in Table 2 and indicate whether they are caused by temporal and/or instrumental effects which we examine further in sections 3.2 and 3.3. Except for the boundary layer, where both temporal and instrumental sampling biases are present, the total sampling biases are mainly due to instrumental effects.

3.2. Temporal Sampling Bias

Figure 3 shows our estimate based on MERRA of the yearly average temperature and water vapor temporal sampling biases of AIRS/AIRS-A climatologies for two levels/layers. A figure with additional levels/layers up to 300 hPa is available in Figure S1 in the supporting information.

As *Fowler et al.* [2000] point out, the largest temporal sampling biases are in regions with a large amplitude in the diurnal cycle. For example, the temporal sampling bias of temperature can be ±2 K in the extratropical boundary layer (Figure 3) because of the large amplitude of the diurnal variation. The water vapor in the tropical and temperate boundary layer over the ocean has a wet temporal sampling bias that can be up to 10% near some coastlines (Figure 3). Similar wet temporal sampling biases in the boundary layer over North America and Northern Eurasia are likely associated with lakes.

The water vapor has both dry and wet temporal sampling biases in the tropical free troposphere (e.g., the 600–500 hPa layer in Figure 3). The largest bias is over the tropical western pacific where *Tian et al.* [2004] show a large amplitude in the diurnal cycle of clouds and upper tropospheric humidity. The direction of the bias likely depends upon whether the AIRS/AMSU-A 1:30 A.M./P.M. equator crossing time captures a peak or trough in the diurnal cycle, therefore other regions show slight wet biases. Nevertheless, both the dry and wet temporal sampling biases in the free troposphere are just a few percent.

We summarize the temporal sampling biases in Table 3. Although the temporal sampling biases are generally small, they are significant and contribute to the observed differences observed when comparing gridded AIRS/AMSU-A data to climate models [e.g., *Tian et al.*, 2013].

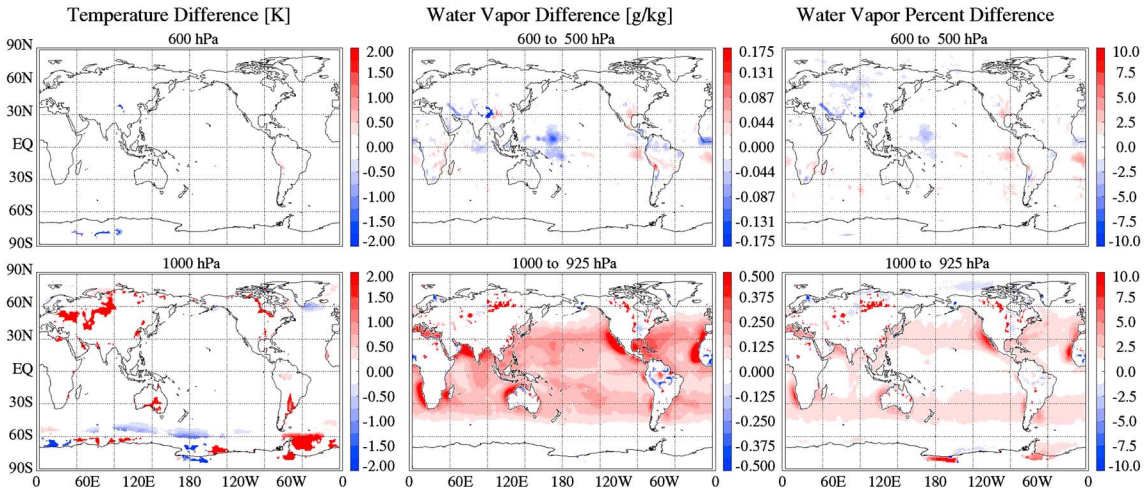

Figure 3. Differences between MERRA sampled Like AIRS/AMSU-A and MERRA Monthly Mean climatologies (i.e., MSA-MMM) of temperature in Kelvins, water vapor in g/kg, and water vapor percent difference are displayed from left to right. This is an estimate of just the temporal component to the sampling bias of an AIRS/AMSU-A climatology.

Table 3. Temporal Sampling Bias Estimates

Region	Bias
Over some extratropical boundary layer regions	± 2 K
Boundary layer above tropical and temperate oceans and lakes	up to 10% wet (larger close to coastlines)
Tropical free troposphere	a few percent wet or dry

The boundary layer temporal sampling biases in Figure 3 look different than those shown in Figure 2 from *Guan et al.* [2013] for several reasons. The main reason for the differences is likely that *Guan et al.* [2013] only account for the AIRS/AMSU-A orbital track and swath width but not the surface pressure of the observations. The figures from *Guan et al.* [2013] show that the largest temporal sampling biases of temperature and water vapor at 1000 hPa are over land, however, 1000 hPa is below the land surface of the Earth for much of the Earth. Also, the temporal sampling bias estimates shown by *Guan et al.* [2013] are based on 6-hourly CFSR (National Centers for Environmental Prediction Climate Forecast System Reanalysis) data while ours are based on 3-hourly MERRA data which *Guan et al.* [2013] show differs from that of CFSR in Taylor diagrams. Finally, *Guan et al.* [2013] do not account for the increase in distance between AIRS/AMSU-A footprints at larger scan angles as we do by gridding the actual AIRS Level 2 footprint locations. Nevertheless, our finding that the orbitally induced temporal sampling biases are small is consistent with *Guan et al.* [2013].

3.3. Instrumental Sampling Bias

Figure 4 displays our estimates based on MERRA of the instrumental sampling biases of AIRS/AMSU-A temperature and water vapor climatologies. The most extensive instrumental sampling biases of both temperature and water vapor (Figure 4) are throughout the troposphere over the midlatitude storm tracks where the instrumental sampling biases can be up to 2 K cold and more than 20% dry. Both the cold and dry biases are larger over ocean. The water vapor also has a dry sampling bias in the free troposphere above 850 hPa over the tropical convective cloudy regions such as the ITCZ and SPCZ, the western Pacific warm pool, equatorial South America, and the South Atlantic Convergence Zone. Since these biases are in regions with a smaller fraction of accepted retrievals (see Figure 1) and have a spatial distribution similar to that of clouds, the clouds are likely causing the more warm and humid data to be rejected by the quality control. This is consistent with *Tian et al.* [2013] who show that the large MERRA-AIRS/AMSU-A specific humidity differences are mainly located in the deep convective cloudy regions where the sampling of AIRS/AMSU-A is very low.

We also observe seasonal and diurnal differences within some regions that have a cloud-induced sampling bias. For example, Figure 5 shows that the oceanic boundary layer at 1000 hPa in the northern temperate zones has a ∼1 K warm bias during the June, July, and August (JJA) season and a ∼1 K cold bias during the December, January, and February (DJF) season. Figures S2 and S3 in the supporting information show that the warm bias during the JJA season is larger during the ascending (daytime) part of the orbit while the cold bias during the DJF season is about the same magnitude for both the ascending (daytime) and descending (nighttime) parts of the orbit. These opposite seasonally dependent sampling biases cancel out and are not seen at 1000 hPa in the yearly average instrumental sampling bias estimates shown in Figure 4. Figure 5 also shows a larger seasonally dependent instrumental sampling bias in the boundary layer over northwestern Eurasia that is ∼2 K warm during the JJA season for the ascending (daytime) part of the orbit. The same region has a ∼2 K cold instrumental sampling bias during the DJF season for both the ascending (daytime) and descending (nighttime) parts of the orbit. At higher altitudes in the troposphere the warm biases over the northern temperate oceans and northwestern Eurasia during the JJA season are smaller or not present, while Figures S2 and S3 in the supporting information show that these regions have a cold bias in the troposphere during other seasons. These biases are likely modulated by the seasonal cycle of the storm tracks since the warm bias occurs during the minimum of storm track variability and the cold bias occurs during the maximum [e.g., *Wettstein and Wallace*, 2010].

Figure 5 also shows a 2 K cold seasonally dependent instrumental sampling bias off the coast of Antarctica during the JJA season that is not present during the DJF season and a similar cold instrumental sampling bias in the Arctic Ocean during the DJF season that is not present during the JJA season. Unlike most other seasonally dependent instrumental sampling biases that are larger when there is a seasonal decrease in the fraction of accepted retrievals, these cold biases are larger when there is a seasonal increase in the fraction of accepted retrievals (not shown). These biases are likely an artifact of how the AIRS/AMSU-A quality control

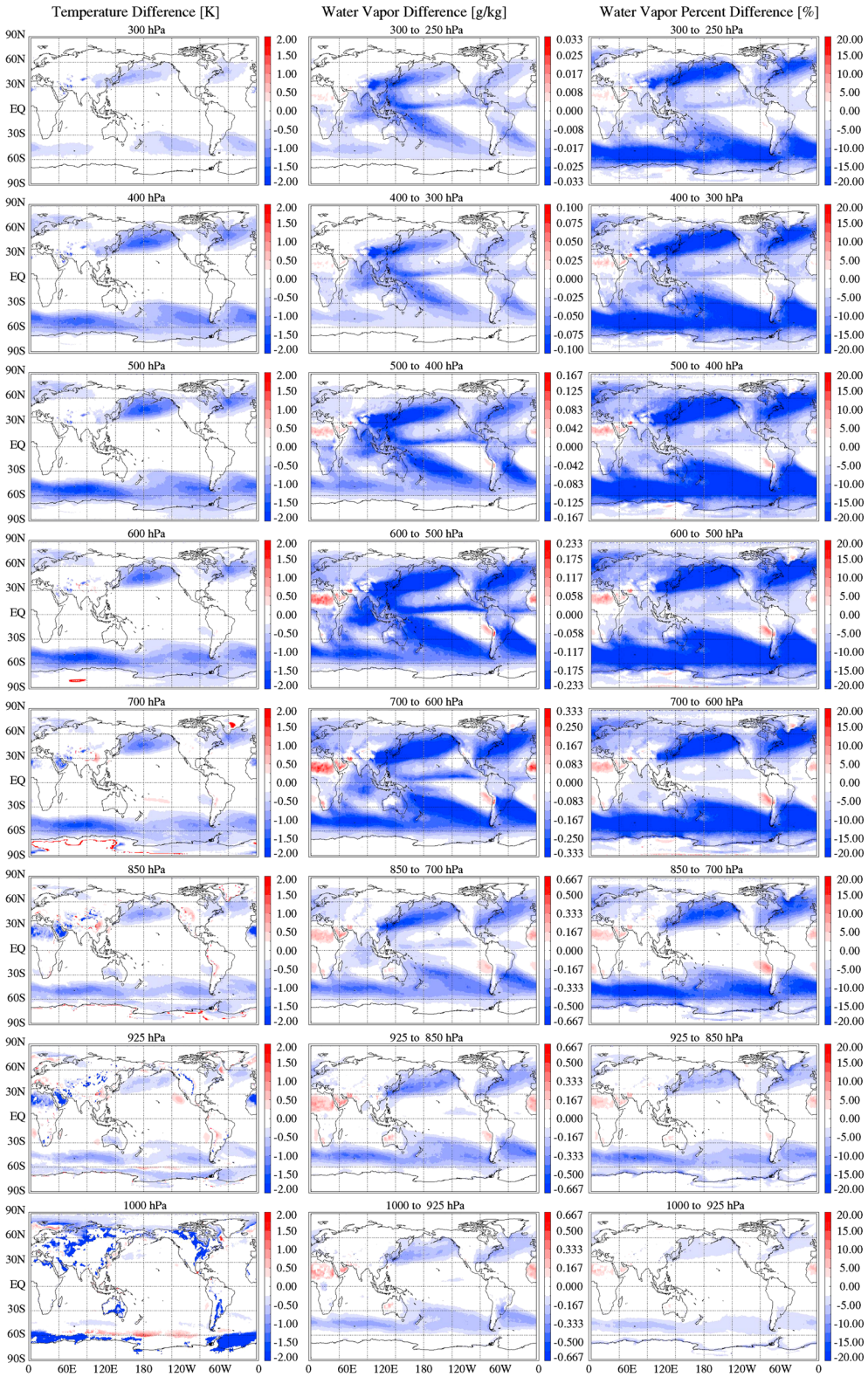

Figure 4. Differences between MERRA sampled Like AIRS/AMSU-A with Quality Control and MERRA sampled Like AIRS/AMSU-A climatologies (i.e., MSAQC-MSA) are shown for air temperature in Kelvins, water vapor mixing ratio in g/kg, and percent difference of water vapor mixing ratio from left to right. This is an estimate of just the instrumental component to the sampling bias of an AIRS/AMSU-A climatology.

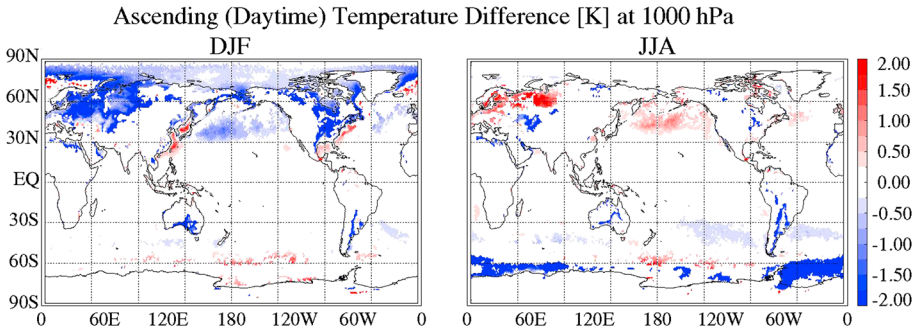

Figure 5. Differences between the MERRA sampled Like AIRS/AMSU-A with quality control-MERRA sampled Like AIRS/AMSU-A climatologies for the ascending part of the orbit for DJF and JJA (MSAQC-A-DJF–MSA-A-DJF and MSAQC-A-JJA–MSA-A-JJA) are shown at for 1000 hPa temperature in Kelvins).

responds to ice-covered surfaces such that during the cold season, although more retrievals are accepted, they tend to be colder than average.

Over the Sahara, Sahel, and the Arabian Peninsula the AIRS/AMSU-A quality control creates a > 1 K cold instrumental sampling bias at 925 and 850 hPa and a wet instrumental sampling bias up to 20% wet that affects all layers of the troposphere (Figure 4). This cold/wet instrumental sampling bias has a strong seasonal dependence such that the largest biases are over the Sahara, Sahel, and the Arabian Peninsula during the March, April, and May (MAM) and JJA seasons and they are more prominent during the ascending (daytime) part of the orbit. Figures S2, S3, S4, and S5 in the supporting information show similar seasonally dependent cold/wet sampling biases over the western part of Australia during the September, October, and November (SON) and DJF seasons. However, over Australia a nighttime dry instrumental sampling bias cancels out the daytime wet bias so that neither are seen in the yearly and diurnally averaged bias estimates in Figure 4. We note that the fraction of accepted retrievals (not shown) in these regions is significantly lower during the daytime observations for the affected seasons than at night or during other seasons. Since there are not many clouds over deserts, these differences may be due to surface emissivity, high surface temperatures, or aerosols affecting the quality flagging such that dry retrievals are rejected throughout the troposphere and warm retrievals are rejected at 925 and 850 hPa.

Smaller seasonal variations in the sampling biases than those described above are correlated with seasonal changes in the number of accepted retrievals. Because of seasonal and diurnal canceling errors these biases can appear smaller in the yearly average. For example, the yearly average sampling biases in Figure 4 shows both temperature and water vapor instrumental sampling biases over the tropical ocean west of South America. At 1000 and 925 hPa the temperature bias appears as a ~0.5 K warm bias while from 850 to 600 hPa it appears as a ~0.5 K cold bias. The troposphere in this region has a consistent wet bias from 925 to 500 hPa that is largest (~10%) in the layer from 850 to 700 hPa. Figures S4 and S5 in the supporting information show that the wet bias off the west coast of South America has a seasonal and diurnal dependence such that it is largest (15% wet) in the layer from 850 to 700 hPa during the SON season at night. The peak in this bias corresponds with a decrease in the ratio of accepted retrievals (not shown).

We summarize the instrumental sampling biases in Table 4. As mentioned earlier, except for the boundary layer, where both temporal and instrumental sampling biases are present, instrumental sampling biases are the main contributor to the total sampling bias.

4. Measurement Uncertainties (AIRS/AMSU-A–MERRA With the Same Sampling)

Tian et al. [2013] show that side-by-side comparisons of yearly climatological means of AIRS/AMSU-A and MERRA temperature and water vapor have good correspondence with both data sets showing similar spatial patterns even without accounting for differences in sampling. They also use the differences between the AIRS/AMSU-A and MERRA climatologies to estimate a combined uncertainty that includes both measurement and sampling uncertainties. In this section we calculate a combined uncertainty estimate for AIRS/AMSU-A and MERRA that only includes measurement differences.

Table 4. Instrumental Sampling Bias Estimates

Region	Bias
Troposphere above temperate zones	Up to 2 K cold and more than 20% dry; more prominent over ocean.
Troposphere above 850 hPa over the ITCZ and SPCZ	Up to 20% dry
Over northern hemispheric temperate oceans ~30–60° N.	Up to 1 K warm during JJA and 1 K cold during other seasons. The warm bias is more prominent in the daytime than at nighttime and largest in the boundary layer. The cold bias is larger at higher altitudes.
Over northwestern Eurasia.	2 K warm during JJA and 2 K cold during DJF. The warm bias is more prominent in the daytime than at night.
Over the Arctic and off the western coast of Antarctica.	Up to 2 K cold (JJA in the Southern Hemisphere; DJF in the Northern Hemisphere). The bias is largest in the boundary layer.
Over the Sahara, Sahel, the Arabian Peninsula, and Australia at 925 and 850 hPa. Only present in the daytime.	1 K cold. More prominent during MAM and JJA in the Northern Hemisphere and SON and DJF in the southern hemisphere.
Entire troposphere over the Sahara, Sahel, the Arabian Peninsula, and Australia. Not seen in the yearly and diurnally averaged differences above 700 hPa over Australia because of a nighttime dry bias.	20% wet. More prominent during the daytime for the MAM and JJA seasons in the northern hemisphere and SON and DJF in the Southern Hemisphere.
Troposphere over Australia during the nighttime.	A few to more than 20% dry. Largest in the free troposphere above 700 hPa.
Troposphere over the ocean off the west coast of South America.	Up to 15% wet. A 0.5 K warm bias at 1000 and 925 hPa and a 0.5 K cold bias at 850–600 hPa. Largest at night during the SON season in the from 850 to 700 hPa.

Figure 6 shows zonal plots of the average difference between AIRS/AMSU-A and MERRA climatologies (AIRS/AMSU-A–MSAQC) of temperature and water vapor with similar sampling. The zonal difference plots in Figure 6 look similar to the inverse of the MERRA-AIRS/AMSU-A zonal difference plots shown by *Tian et al.* [2013, Figures 2 and 3]. However, Figure 6 of this paper shows smaller differences of both temperature and water vapor in the free troposphere of the temperate zones because the sampling biases of AIRS/AMSU-A climatologies have been accounted for in the MSAQC climatology.

In the tropics and subtropics the zonal average differences in Figure 6 show that the AIRS/AMSU-A climatologies are ~1 K colder than MERRA at 300 hPa. The AIRS/AMSU-A temperature climatology matches MERRA very well in the tropical free troposphere from 600 to 400 hPa. Below that, the differences alternate such that the AIRS/AMSU-A climatology is ~0.7 K warmer than MERRA at 700 hPa, ~0.5 K colder than MERRA at 850 hPa, and ~0.5 K warmer than MERRA again at 925 hPa.

Figure 6 also shows that the AIRS/AMSU-A water vapor climatology is ~20% drier than MERRA in the tropical free troposphere above 700 hPa and is on average ~12% wetter than MERRA in the tropics and subtropics in the layer from 925 to 850 hPa (Figure 6). However, the global maps of AIRS/AMSU-A–MSAQC in Figure 7 show that there are some regions over land and to the west of tropical South America in the layer from 925 to 850 hPa where the AIRS/AMSU-A climatology is drier than MERRA. These differences cancel each other out in the zonally averaged difference maps. Neglecting the dry regions, the AIRS/AMSU-A climatology is up to 30% wetter than MERRA in the band around Earth in the layer from 925 to 850 hPa.

In the layer from 850 to 700 hPa, just above the dry region to the west of South America, the AIRS/AMSU-A climatology is ~25% wetter than MERRA. Although this region has a tendency for downwelling air, we do

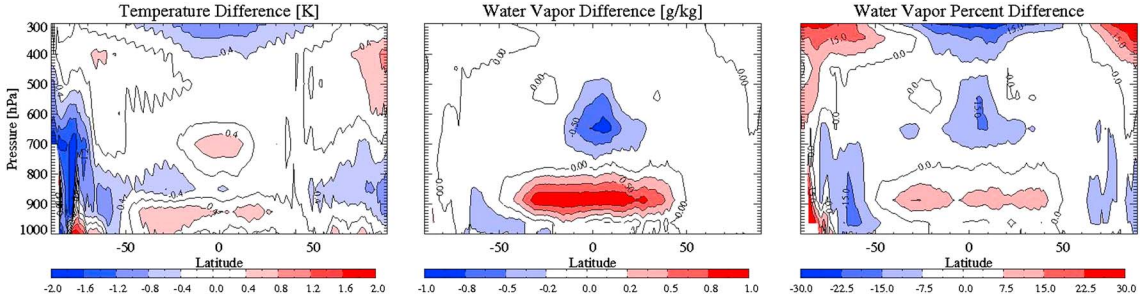

Figure 6. Zonally averaged differences between similarly sampled AIRS/AMSU-A and MERRA (AIRS/AMSU-A–MERRA sampled like AIRS/AMSU-A [MSAQC]) climatologies of (left) air temperature in Kelvins, (middle) water vapor mixing ratio in g/kg, and (right) percent difference of water vapor mixing ratio. These differences are an estimate of the combined measurement uncertainty of AIRS/AMSU-A and MERRA at the locations where AIRS/AMSU-A is able to obtain observations. We have not applied a significance test to these differences.

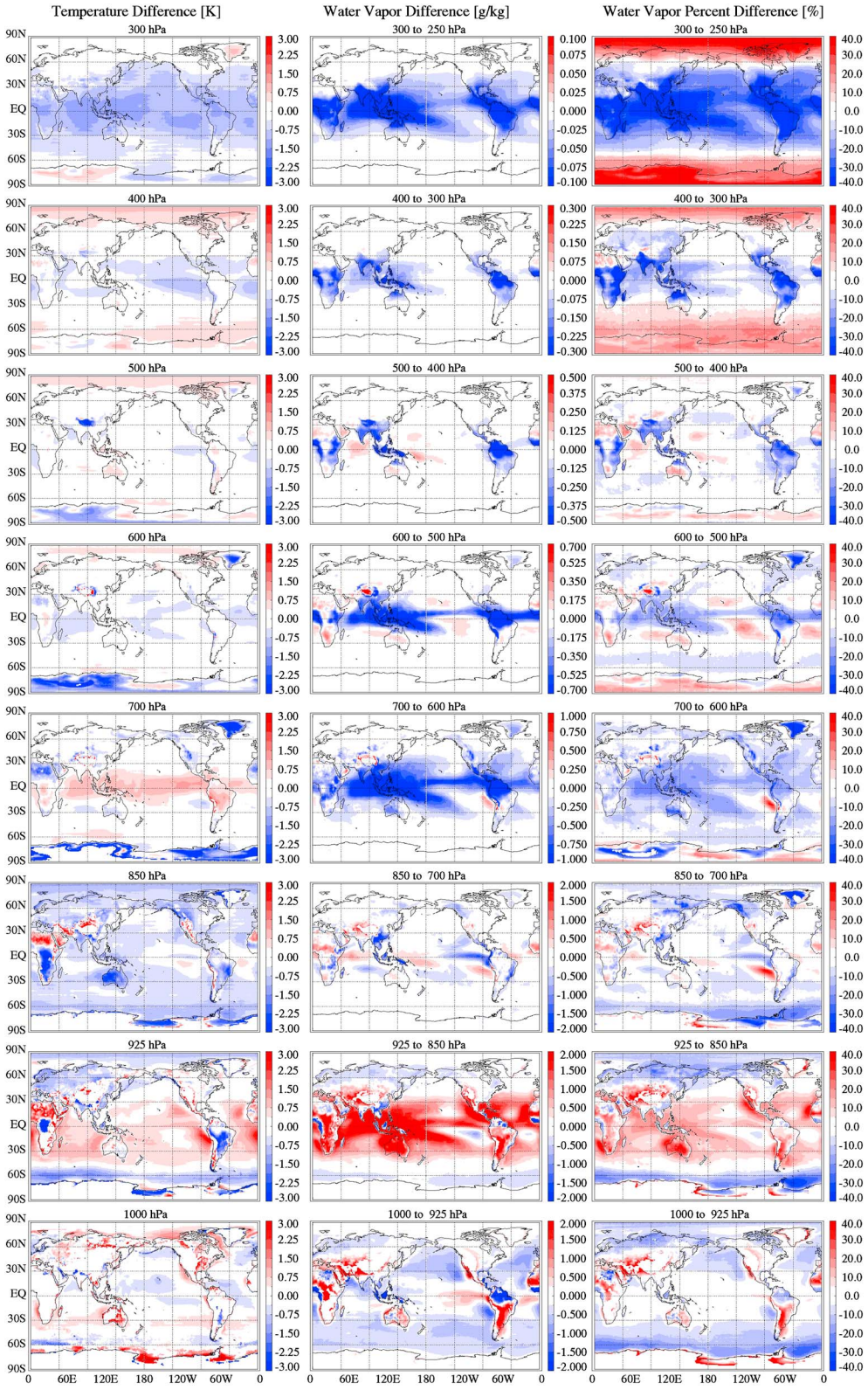

Figure 7. Differences between similarly sampled AIRS/AMSU-A and MERRA (AIRS/AMSU-A–MERRA sampled like AIRS/AMSU-A [MSAQC]) climatologies of air temperature in Kelvins, water vapor mixing ratio in g/kg, and percent difference of water vapor mixing ratio, from left to right. These differences are an estimate of the combined measurement uncertainty of AIRS/AMSU-A and MERRA at the locations where AIRS/AMSU-A is able to obtain observations.

Table 5. Measurement Uncertainty Estimates

Region	Differences[a]
Tropics at ~300 hPa	~1 K colder and 20% drier
Tropical free troposphere between 700 and 500 hPa and above 400 hPa over the ITCZ and SPCZ	20% drier
Over tropical ocean	Up to 0.7 K warmer at 700 hPa, 0.5 colder at 850 hPa, 0.5 warmer at 925 hPa
Band around the Earth in the tropics and subtropics ~925–850 hPa	Up to 30% wetter
Arctic and Antarctic at elevations below 700 hPa	Up to 1–2 K colder
Over the Antarctic ice sheets at 1000 hPa	> 2 K warmer
Arctic and Antarctic above 400 hPa	20–40% wetter
Over Sahara ~700 hPa	1 K colder
Over Sahara 925–850 hPa	2 K warmer
West of South America and Africa at 925–850 hPa	A few percent drier
West of South America and Africa at 850–700 hPa	~25% wetter
Over southern South America	Up to 30% wetter
Oceanic boundary layer 1000–925 hPa except for some regions in the tropics	Up to 20% drier

[a] AIRS/AMSU-A climatology relative to MERRA climatology.

not know whether AIRS/AMSU-A is too wet or MERRA is too dry. However, we note that AIRS/AMSU-A also reports larger cloud top pressures than MERRA in this region (not shown).

In the Arctic and Antarctic the AIRS/AMSU-A climatology is ~1–2 K colder than MERRA at elevations below 700 hPa. Since *Wang et al.* [2013] also find that AIRS/AMSU-A observations are systematically colder than dropsonde data up to 100 hPa over Antarctica, the MERRA data may better match the dropsonde observations at elevations below 700 hPa while AIRS/AMSU-A and MERRA have similar measurement biases at elevations above this.

Over the Antarctic ice sheets Figure 7 shows that the yearly average temperature of AIRS/AMSU-A at 1000 hPa is more than 2 K warmer than MERRA. Although this could be due to an emissivity problem in the AIRS/AMSU retrievals, a comparison of AIRS/AMSU-A and MODIS surface temperature estimates [*Lee et al.*, 2013] shows that in regions of sea ice MODIS can be up to 12 K warmer than AIRS/AMSU-A which would suggest that the differences between MODIS and MERRA would be even larger in these regions. We think a more likely explanation is that there is a problem in the boundary layer temperatures either in the AIRS/AMSU-A or MERRA data. Although they do not include MERRA in their study, *Pavelsky et al.* [2011] find that reanalyses and climate models tend to find stronger inversions over sea ice than AIRS which is consistent with Figure 7 that shows warmer temperatures for AIRS/AMSU-A at 1000 hPa. Nevertheless, further validation of both data sets should be performed in these regions.

Since there is not much water vapor in the arctic and antarctic, the magnitudes of the differences between the AIRS/AMSU-A and MERRA water vapor (Figure 6, middle) are small relative to the tropics, however, the percent difference (Figure 6, right) shows that AIRS/AMSU-A is 20–40% wetter than MERRA at altitudes above 400 hPa in the arctic. Since AIRS/AMSU-A has no skill in measuring stratospheric water vapor (*Liang et al.* [2010]) and the tropopause can sometimes be low over the poles [e.g., *Holton et al.*, 1995], these differences could be due to erroneous stratospheric water vapor estimates from AIRS.

The zonal figure (Figure 6) suggests that the AIRS/AMSU-A water vapor climatology is up to 20% drier than MERRA in the southern ocean boundary layer ~40–70° south latitude. However, Figure 7 shows that the AIRS/AMSU-A climatology is drier than MERRA in the boundary layer from 1000 to 925 hPa over most of the ocean except for a few regions near the equator to the west of continents. The dry differences over the ocean in other regions are canceled out in the zonal averages by wet differences over land.

Canceling errors can also arise in differences between global maps of data sets that have different sampling. An example of this can be seen over the Sahara, Sahel, and the Arabian Peninsula where *Tian et al.* [2013, Figure 7] suggests that the AIRS/AMSU-A climatology is colder than MERRA at 850 and 700 hPa and there are no differences at 925 hPa. However, Figure 7 from this paper shows that while the AIRS/AMSU-A climatology is colder than MERRA at 700 hPa it is warmer than MERRA at both 925 and 850 hPa when both data sets are sampled similarly. The cold instrumental sampling bias at 925 and 850 hPa (see section 3) likely negates the warm measurement difference at these levels, which leads to the incorrect interpretation of the measurement differences when the sampling differences are neglected. These measurement and

sampling differences over desert regions could be due to emissivity errors [*Hulley et al.*, 2009] that affect both the retrievals and the quality screening.

Another notable feature in Figure 7 is that over the ITCZ and SPCZ the AIRS/AMSU-A climatology is 20% drier than the MERRA climatology in the layers from 700 to 500 hPa and in the layers above 400 hPa while the layers between and below these AIRS/AMSU-A climatology is wetter than MERRA climatology. This could indicate that deep convective clouds in these regions are causing a bias the retrievals even though the data pass the quality control criteria or that these regions are not properly characterized in the MERRA data.

The AIRS/AMSU-A water vapor tends to be as much as 30% wetter than MERRA in the 1000–925 hPa layer over southern South America (see Figure 7). This is consistent with *Trenberth et al.* [2011] who show that MERRA is systematically dryer than European Centre for Medium-Range Weather Forecasts Reanalysis Interim (ERA-Interim) data over southern South America and note that MERRA has major problems in this region. Also, *Lorenz and Kunstmann* [2012] find that significant discrepancies exists between the precipitation patterns from Global Precipitation Climatology Centre, ERA-Interim, and MERRA over South America. We summarize the measurement uncertainties in Table 5.

5. Limitations of this Study and Future Work

Before discussing our conclusions we point out several important caveats to our analysis and potential figure studies. We use MERRA data to estimate the sampling biases of AIRS/AMSU-A derived temperature and water vapor climatologies given the assumption that MERRA has information where AIRS/AMSU-A does not. However, in section 4 we show that even when MERRA is sampled similarly to AIRS/AMSU-A the differences are often larger than the sampling biases. Since MERRA may also not be able to correctly represent the atmospheric state in regions where AIRS is not able to perform successful retrievals, our sampling bias estimates could be flawed. The MERRA is strongly influenced by the data it assimilates. If it does not have observations to assimilate in a particular region, it will rely more on the GEOS-5 model. Therefore, in future studies we intend to perform similar studies using other reanalyses such as ERA-Interim or CFSR which might better represent the diurnal cycle in certain regions because of more frequent diurnal sampling. Nevertheless, since there are still large discrepancies among different reanalyses particularly with respect to the hydrological cycle [e.g., *Trenberth et al.*, 2011; *Lorenz and Kunstmann*, 2012] caution should be used when interpreting results from any of these analyses.

Another caveat is that MERRA assimilates AIRS/AMSU-A clear sky radiances. Although this probably has little effect on our sampling bias estimates, since assimilation data are sensitive to the data they use [e.g., *English et al.*, 2000], it may cause an underestimate of the combined measurement uncertainties based on the differences between AIRS/AMSU-A and MERRA. However, since MERRA only assimilates a small number (< 1%) of the available AIRS/AMSU-A clear sky radiances using an algorithm similar to that described by *Le Marshall et al.* [2006] (R. Gelaro, personal communication, 2013) we expect this effect to be small.

Also, the MSAQC and MSA climatologies are not sampled exactly like AIRS. The MERRA data are provided on a 1.25° × 1.25° grid with 42 vertical levels in pressure and sampled every 3 h in time. We use the nearest MERRA profile in space and time and interpolate the MERRA water vapor profile in pressure to simulate the AIRS/AMSU-A water vapor layers. Errors due to interpolation or subgridscale variability could cause an overestimate of the uncertainty when comparing similarly sampled AIRS/AMSU-A and MERRA climatologies.

We also point out that these sampling bias estimates are for AIRS, an infrared instrument on the Aqua spacecraft, which is in a Sun-synchronous orbit with a 1:30 A.M./P.M. equator crossing time. Although our conclusions might be applicable to other infrared instruments, even an instrument exactly like AIRS/AMSU-A in a different Sun-synchronous orbit might have different instrumental and temporal components to the sampling bias. Also, we show the sampling biases based on averages over 9 years of observations. Because of the limited swath width of AIRS we expect that the temporal sampling biases are larger for any given daily or monthly average because regions with large spatial or synoptic variability may not be sufficiently sampled at shorter time scales.

We show in this paper that averaging over the ascending (day) and descending (night) parts of the AIRS/AMSU-A orbit and averaging over different seasons can cause sampling biases to cancel out. Similar diurnally or seasonally dependent measurement differences may also cause errors in our combined mea-

surement uncertainties of AIRS/AMSU-A and MERRA climatologies. We plan to investigate these differences in a subsequent paper focusing on the seasonal and diurnal differences between AIRS/AMSU-A and MERRA.

6. Conclusions

We investigate the magnitude of the sampling biases of AIRS/AMSU-A temperature and water vapor climatologies by calculating the differences between MERRA climatologies created with different sampling as described in Table 1. These differences enable us to calculate the total sampling bias and separate it into two components. The temporal component to the sampling bias is caused by the Aqua space craft's Sun-synchronous low Earth orbit and limited swath width. The instrumental component is caused by certain scenes for which retrievals are not possible or they are rejected by the quality control.

Consistent with previous studies [e.g., *Guan et al.*, 2013; *Fowler et al.*, 2000], we find that the temporal sampling biases are relatively small compared to the instrumental sampling biases and measurement uncertainties. Nevertheless, the temporal sampling biases can be statistically significant in regions with a large diurnal variation such as the boundary layer and certain regions in the tropical troposphere. The temporal sampling biases of temperature are only significant in the boundary layer. We find wet temporal sampling biases in the tropical boundary layer and both wet and dry temporal sampling biases in the tropical free troposphere in regions with a large diurnal variation. The bias can be both wet and dry depending upon which phase of the diurnal cycle is sampled by the AIRS/AMSU-A 1:30 A.M./P.M. equator crossing time. The temporal sampling biases we show would be experienced by any Earth observing instrument in a Sun-synchronous low Earth orbit with a 1:30 A.M./P.M. equator crossing time (e.g., other instruments on Aqua or Suomi) although they could be larger or smaller depending upon the swath width.

Instrumental sampling biases are caused by atmospheric or environmental conditions (e.g., uniform or thick clouds, warm scenes, Sun glint) that prevent the instrument or algorithm from successfully retrieving the atmospheric state. Therefore, the instrumental sampling biases tend to be larger and more varied than the temporal sampling biases. Although the instrumental sampling biases of an AIRS/AMSU-A derived climatology are often small compared to other sources of error such as the measurement uncertainties, they can be large in specific geographic regions and can influence comparisons with differently sampled data sets. For example, instrumental sampling accounts for most of the tropospheric cold/dry bias in the temperate zones over storm tracks and much of the dry bias over the tropical deep convective regions, such as the Intertropical Convergence Zone and the South Pacific Convergence Zone. Clouds are the likely main cause of these biases since there is a reduction in the fraction of accepted retrievals in these regions that resembles the distributions of cloudy regions. However, other factors such as surface emissivity and surface temperature can also influence the instrumental sampling bias over deserts where the biases can be up to 1 K cold and 10% wet. Some instrumental sampling biases can vary seasonally and/or diurnally. Except for the boundary layer, where both temporal and instrumental sampling biases are present, the total sampling biases are mainly from the instrumental sampling biases.

Sampling biases can lead to erroneous conclusions when comparing differently sampled data sets or averaging over different seasons or parts of the orbit. For example, we show a cold instrumental sampling bias over deserts masks a warm measurement difference when sampling differences are not considered. Also, averaging the AIRS/AMSU-A data over the ascending (daytime) and descending (nighttime) parts of the orbit cancels out some sampling biases. During DJF season we find a wet instrumental sampling bias over Australia in the daytime and a dry instrumental sampling bias at night that cancel each other out in the yearly and diurnally averaged sampling bias estimates. Similar instrumental sampling biases to what we show likely exist for climatologies derived from other infrared instruments (e.g., IASI, CrIS, and MODIS) that are not be able to perform retrievals under all observing conditions. Since these sampling differences can be significant they should be considered when performing intercomparisons of satellite observations with regularly gridded data sets like climate models.

In order to separate measurement differences from the sampling differences, we compare temperature and water vapor climatologies derived from similarly sampled AIRS/AMSU-A and MERRA measurements. While the uncertainties in the current generation of climate models are larger than the combined uncertainties of AIRS/AMSU-A and MERRA even without accounting for the differences in sampling [e.g., *Tian et al.*, 2013], as the models improve, more careful intercomparisons will be necessary.

Also, the differences between similarly sampled AIRS/AMSU-A and MERRA temperature and water vapor climatologies are smaller than when sampling differences are neglected (*Tian et al.* [2013]); however, there are still significant measurement differences between the AIRS/AMSU-A and MERRA data (Figure 7).

In the tropical upper troposphere the AIRS/AMSU-A climatology tends to be colder and drier than the MERRA climatology. AIRS is also drier than MERRA in the tropical free troposphere above 700 hPa. Although the AIRS/AMSU-A climatology is generally wetter than MERRA in the ~925–850 hPa layer in the tropics, there are regions within this band over land and over the Pacific Ocean to the west of tropical South America where AIRS/AMSU-A is drier. In the arctic and antarctic the AIRS/AMSU-A climatology is ~1–2 K colder than MERRA at elevations below 700 hPa except over the antarctic ice sheets where the AIRS/AMSU-A climatology is ~2 K warmer than MERRA. Also, in the arctic and antarctic the AIRS/AMSU-A climatology is ~30% wetter than MERRA at elevations above 400 hPa. The measurement differences between AIRS/AMSU-A and MERRA could be caused by a number of deficiencies in either data set such as assumptions about the surface type, paucity of assimilation data, or artifacts of cloud clearing. Further studies of the regions where there are significant differences between the AIRS/AMSU-A and MERRA climatologies should be performed to improve the observations and to determine the locations where either the AIRS/AMSU-A or the MERRA observations are better suited to evaluate climate models.

Acknowledgments

T.H. wishes to acknowledge conversations with Gregory Leptoukh as an early impetus for this work. Also, Ron Gelaro, Mike Bosilovich, Peter Smith, and Dana Ostrenga provided insights into the MERRA data. Glynn Hulley, Suhung Shen, and Zhanqing Li helped us to understand some of the atmospheric and surface phenomena discussed in this paper. John Blaisdel and Joel Susskind helped us to understand aspects of the AIRS/AMSU-A retrieval algorithm relevant to this study. We also acknowledge three anonymous referees who helped us to improve this paper and suggested ideas for future studies. Part of this research was performed at the Jet Propulsion Laboratory (JPL), California Institute of Technology (Caltech), under a contract with the National Aeronautics and Space Administration (NASA). The AIRS/AMSU-A and MERRA data presented in this paper are available from Goddard Earth Sciences Data and Information Services Center (GES DISC; disc.gsfc.nasa.gov).

References

Aumann, H. H., et al. (2003), AIRS/AMSU/HSB on the Aqua mission: Design, science objectives, data products and processing system, *IEEE Trans. Geosci. Remote Sens.*, *41*, 253–264.

Bell, T. L., and P. K. Kundu (1996), A study of the sampling error in satellite rainfall estimates using optimal averaging of data and a stochastic model, *J. Clim.*, *9*, 1251–1268.

English, S. J., R. J. Renshaw, P. C. Dibben, A. J. Smith, P. J. Rayer, C. Poulsen, F. W. Saunders, and J. R. Eyre (2000), A comparison of the impact of TOVS and ATOVS satellite sounding data on the accuracy of numerical weather forecasts, *Q. J. R. Meteorol. Soc.*, *126*, 2911–2931.

Fasullo, J. T., and K. E. Trenberth (2012), A less cloudy future: The role of subtropical subsidence in climate sensitivity, *Science*, *338*, 792–794.

Fetzer, E. J., B. H. Lambrigtsen, A. Eldering, H. H. Aumann, and M. T. Chahine (2006), Biases in total precipitable water vapor climatologies from Atmospheric Infrared Sounder and Advanced Microwave Scanning Radiometer, *J. Geophys. Res.*, *111*(9), D09S16, doi:10.1029/2005JD006598.

Fowler, L. D., B. A. Wielicki, D. A. Randall, M. D. Branson, G. G. Gibson, and F. M. Denn (2000), Use of a GCM to explore sampling issues in connection with satellite remote sensing of the Earth radiation budget, *J. Geophys. Res.*, *105*, 20,757–20,772, doi:10.1029/2000JD900239.

Guan, B., D. Waliser, J. Li, and A. da Silva (2013), Evaluating the impact of orbital sampling on satellite—climate model comparisons, *J. Geophys. Res. Atmos.*, *118*, 355–369, doi:10.1029/2012JD018590.

Holton, J. R., P. H. Haynes, M. E. McIntyre, A. R. Dougla, R. B. Roo, and L. Pfister (1995), Stratosphere-troposphere exchange, *Rev. Geophys.*, *33*, 403–439.

Hulley, G. C., S. J. Hook, E. Manning, S.-Y. Lee, and E. Fetzer (2009), Validation of the Atmospheric Infrared Sounder (AIRS) version 5 land surface emissivity product over the Namib and Kalahari Deserts, *J. Geophys. Res.*, *114*, D19104, doi:10.1029/2009JD012351.

John, V. O., G. Holl, R. P. Allan, S. A. Buehler, D. E. Parker, and B. J. Soden (2011), Clear-sky biases in satellite infrared estimates of upper tropospheric humidity and its trends, *J. Geophys. Res.*, *116*, D14108, doi:10.1029/2010JD015355.

Kirk-Davidoff, D. B., R. M. Goody, and J. G. Anderson (2005), Analysis of sampling errors for climate monitoring satellites, *J. Clim.*, *18*, 810–822.

Lee, Y.-R., J.-M. Yoo, M.-J. Jeong, Y.-I. Won, T. Hearty, and D.-B. Shin (2013), Comparison between MODIS and AIRS/AMSU satellite-derived surface skin temperatures, *Atmos. Meas. Tech.*, *6*, 445–455, doi:10.5194/amt-6-445-2013.

Le Marshall, J., et al. (2006), Improving global analysis and forecasting with AIRS, *Bull. Am. Meteorol. Soc.*, *87*, 891–894, doi:10.1175/BAMS-87-7-891.

Leroy, S. S. (2001), The effects of orbital precession on remote climate monitoring, *J. Clim.*, *14*, 4330–4337.

Liang, C. K., A. Eldering, F. W. Irion, W. G. Read, E. J. Fetzer, B. H. Kahn, and K.-N. Liou (2010), Characterization of merged AIRS and MLS water vapor sensitivity through integration of averaging kernels and retrievals, *Atmos. Meas. Tech. Discuss.*, *3*, 2833–2859.

Lin, X., L. D. Fowler, and D. A. Randall (2002), Flying the TRMM Satellite in a general circulation model, *J. Geophys. Res.*, *107*(D16), 4281, doi:10.1029/2001JD000619.

Lorenz, C., and H. Kunstmann (2012), The hydrological cycle in three state-of-the-art reanalyses: Intercomparison and performance analysis, *J. Hydrometeorol.*, *13*, 1397–1420.

North, G. R., S. S. P. Shen, and R. Upson (1993), Sampling errors in rainfall measurements by multiple satellites, *J. Appl. Meteorol.*, *32*, 399–410.

Olsen, E., S. Granger, E. Manning, and J. Blaisdell (2007), *AIRS/AMSU/HSB Version 5 Level 3 Quick Start*, Jet Propulsion Laboratory California Institute of Technology, Pasadena, Calif.

Parkinson, C. L. (2003), Aqua: An Earth-observing satellite mission to examine water and other climate variables, *IEEE Trans. Geosci. Remote Sens.*, *41*(2), 173–183.

Pavelsky, T. M., J. Boé, A. Hall, and E. J. Fetzer (2011), Atmospheric inversion strength over polar oceans in winter regulated by sea ice, *Clim. Dyn.*, *36*, 945–955.

Rienecker, M. M., et al. (2011), MERRA: NASA's Modern-Era retrospective analysis for research and applications, *J. Clim.*, *24*, 3624–3648, doi:10.1175/JCLI-D-11-00015.1.

Rossow, W. B., and R. A. Schiffer (1991), ISCCP cloud data products, *Bull. Am. Meteorol. Soc.*, *72*, 2–20.

Susskind, J., C. D. Barnet, and J. M. Blaisdell (2003), Retrieval of atmospheric and surface parameters from AIRS/AMSU/HSB data in the presence of clouds, *IEEE Trans. Geosci. Remote Sens.*, *41*(2), 390–409.

Susskind, J., C. Barnet, J. Blaisdell, L. Iredell, F. Keita, L. Kouvaris, G. Molnar, and M. Chahine (2006), Accuracy of geophysical parameters derived from Atmospheric Infrared Sounder/Advanced Microwave Sounding Unit as a function of fractional cloud cover, *J. Geophys. Res.*, *111*(D9), D09S17, doi:10.1029/2005JD006272.

Susskind, J., J. M. Blaisdell, L. Iredell, and F. Keita (2011), Improved temperature sounding and quality control methodology using AIRS/AMSU data: The AIRS science team version 5 retrieval algorithm, *IEEE Trans. Geosci. Remote Sens.*, *49*, 883–907, doi:10.1109/TGRS.2010.2070508.

Tian, B., B. J. Soden, and X. Wu (2004), Diurnal cycle of convection, clouds, and water vapor in the tropical upper troposphere: Satellites versus a general circulation model, *J. Geophys. Res.*, *109*, D10101, doi:10.1029/2003JD004117.

Tian, B., E. Fetzer, B. Kahn, J. Teixeira, E. Manning, and T. Hearty (2013), Evaluating CMIP5 models using AIRS tropospheric air temperature and specific humidity climatology, *J. Geophys. Res. Atmos.*, *118*, 114–134, doi:10.1029/2012JD018607.

Trenberth, K. E., J. T. Fasullo, and J. Mackaro (2011), Atmospheric moisture transports from ocean to land and global energy flows in reanalyses, *J. Clim.*, *24*, 4907–4924.

Wang, J., T. Hock, S. A. Cohn, C. Martin, N. Potts, T. Reale, B. Sun, and F. Tilley (2013), Unprecedented upper-air dropsonde observations over Antarctica from the 2010 Concordiasi Experiment: Validation of satellite-retrieved temperature profile, *Geophys. Res. Lett.*, *40*, 1231–1236, doi:10.1002/grl.50246.

Wettstein, J. J., and J. M. Wallace (2010), Observed patterns of month-to-month storm track variability and their relationship to the background flow, *J. Atmos. Sci.*, *67*, 1420–1437.